



OPEN

Enhanced thermal effectiveness for electroosmosis modulated peristaltic flow of modified hybrid nanofluid with chemical reactions

Arafat Hussain¹, Jun Wang^{1✉}, Yasir Akbar² & Riaz Shah²

In this analysis, the thermal and flow properties of modified hybrid nanofluids (MNFs) have been investigated under the effects of electroosmosis and homogeneous-heterogeneous chemical reactions. Three types of nanoparticles of Cu , CuO , and Al_2O_3 are utilized to monitor the performance of the MNFs with water as a working liquid. The determination of the heating phenomenon is explored by incorporating the effects of NPs shape, temperature reliant viscosity, Joule heating, heat generation/absorption and viscous dissipation. In this exploration, equal diffusion factors for the auto catalyst and reactants are assumed. The model formulation contains a highly non-linear PDE system, which is converted to ODEs under physical assumptions with lubrication and Debye–Huckel. The solution treatment involves the Homotopy perturbation method for solving the governing differential equations is used. A major outcome discloses that an addition in heterogeneous reaction parameter aids in enhancing the concentration profile. In a result, the temperature curve decreases at increasing volume fraction of the NPs. Modified hybrid NFs have higher heat transfer rate as compared to base H_2O , or ordinary $Al_2O_3-H_2O$ and hybrid $Cu + Al_2O_3-H_2O$ NFs. Pressure gradient decreases by improving electroosmotic parameter. Further a comparison between analytically (HPM) and numerical results (NDSolve) show that both results are in good agreement.

Abbreviations

\vec{J}	Current density
ϕ_3	Volume fraction of Al_2O_3 nanoparticles
β_f	Thermal expansion coefficient of fluid
δ	Wave number
ϕ_2	Volume fraction of Cu nanoparticles
g	Acceleration due to gravity
σ_f	Electric conductivity of fluid
ε	Dimensionless heat generation/ absorption parameter
T_w	Temperature at channel wall
p	Dimensionless pressure
T_0	Temperature of wall
F	Dimensionless flow rate in wave frame
Pr	Prandtl number
Re	Reynolds number
Br	Brinkman number
Ec	Eckert number
ρ_f	Density of fluid
Gr	Grashoff number
M	Hartman number
θ	Dimensionless temperature
ψ	Stream function
\vec{B}	Applied magnetic field

¹Institute of Applied System Analysis, Jiangsu University, Zhenjiang 212013, Jiangsu, People's Republic of China. ²Department of Mathematics, COMSATS University Islamabad, Islamabad, Pakistan. ✉email: wangmath2011@126.com

\vec{E}	Applied electric field
ϕ_1	Volume fraction of <i>Cuo</i> nanoparticles
T	Dimensional temperature
Φ	Dimensional heat generation/absorption parameter
η	Dimensionless flow rate in laboratory frame

Heat transport is considered one of the main and crucial phenomena in different areas of technologies. The thermal dynamics of nanofluids (NFs) is extremely exciting and new in terms of applications. NFs, an inevitable class of fluid with exceptional heat transfer capability due to suspended nanoscale particles in the base fluid. NFs alludes to a consistent mixture of minute metal particles (5–100 nm) with working liquids such as kerosene, water, oils, EG etc. The resulting liquids, called NFs, have excellent thermal conductivity^{1–3}, uniformity, high stability, and low fouling, making them a universally used medium in various activities, embracing automotive, power generation, extrusion machinery, chemical production, solar collectors, air purifiers, electronics, nuclear systems, and drug therapy. Experimental studies also suggest that the TC of NFs depends on a range of aspects, such as volume fraction of particles, particle size, particle structure, base liquid material, clustering, additives, temperature, and acidity of the NFs^{4,5}. In the nanoliquid size spectrum, the particle surface to particle volume ratio is so large that any interactions are driven by short-range forces such as surface forces and van der Waals attraction. Buongiorno⁶ investigated convective nanofluidic transportation while incorporating Brownian motion and thermophoresis into account. In his research, he noticed that Brownian and thermophoretic diffusion are key factors for extraordinary increase in heat transfer by the NFs. Tiwari and Das⁷ fashioned NFs transportation by entering the size of tiny materials, thermal conductivity, viscosity, and volume fraction into the NFs heat transfer mechanism. Lazarus⁸ addressed the applications of NFs in different heat transfer phenomena. Few recent studies conducted in this direction may also be observed through references^{9–14}.

Oscillations due to transverse translational waves transmitting through a flexible wall led to uninterrupted periodic oscillations of muscle conductors, called peristalsis. This kind of flow is produced by a progressive wave moving from low pressure to high pressure along the tract boundaries under the action of a pump. Peristaltic flow is a phenomenon of natural transport in which body fluid moves from one location to another by continuous relaxation and muscle contraction. Peristaltic movement during the lubrication procedure has been extensively discussed by Shapiro et al.¹⁵. Akram et al.¹⁶ researched ramifications of nanoliquid on peristaltic transportation through an asymmetric channel. Abbasi et al.¹⁷ examined the second law analysis for peristaltic movement of H₂O based nanoliquid. Analytical solution for the resulting system is obtained using HPM. Akbar et al.¹⁸ explored the implications of Hall current and radiative heat flux on peristaltic transportation of nanoliquid with irreversibility rate. Reddy et al.¹⁹ investigated the entropy rate for the gold-blood NFs flow in a microchannel.

Many chemical reactions occurring in various biological and physical phenomena occur in the presence of a catalyst²⁰. The procedure is accelerated by using a catalyst without using it. Due to the physical state of substances, two chemical reactions occur, i.e., homogeneous, and heterogeneous chemical reactions. In addition, these reactions are classified as single phase (gas, liquid and solid) and are called homogeneous reactions, while heterogeneous reactions occur at two or more phases when one or more reactants undertake chemical modifications such as (liquid, solid, solid and gas,). Some reactions are unable to proceed on their own or are conducted with the participation of any catalyst. Several analyses are published on chemical reactions for different uses^{21–23}.

Electroosmotic flow (EOF) relative to a fixed charged surface is the movement of an ionized fluid under the impact of an applied potential or an external electric field. This impact has continued to receive much attention in recent decades due to its application in micropumps, small scale liquid handling, and efficient design of mass and heat transfer systems. Some of the pioneering results in the field of microfluidics are the evolution of inkjet printheads, DNA chip sequencing, drug supply for cancer patients, lab-on-a-chip technologies, and microthermal technologies. Such applications, which include soil conditioning and microscale chemical separation, have encouraged many scientists to research electroosmotic flow in micro geometries over the years. A few representative debates on electroosmosis have been conducted in the investigations^{24–34}.

Inspired by the previously mentioned inspirations, the present pursuit aims to investigate the efficiency of heat transfer and flow of modified hybrid nanofluid under the effects of heterogeneous and homogeneous chemical reactions, temperature-dependent viscosity, electric and magnetic fields, and heat generation/absorption. In addition, shape aspects are also being studied for the nanomaterials used. The MNPs are composed of three forms of nanomaterials, i.e., *Cu*, *Al₂O₃* and *CuO*, NPs which are used to evaluate thermal performance. Basic assumptions are used to design defining expressions for the flow model. The analytical computation using Homotopy Perturbation Method (HPM) is performed for solution procedure. A comprehensive analysis of the corresponding parameters on the flow properties, thermal aspects of nanomaterials and shape features are described and reflected through graphs and tables.

Problem formulation

Here the flow of an electrically conductive modified hybrid nanofluid i.e., *Al₂O₃*, *CuO*, *Cu* nanomaterials, suspended in aqueous (water) ionic solution, which is propelled by the combined effects of electroosmosis and dissemination of sine waves along the entire length of the channel walls with a constant speed *c* is considered. We assumed that the walls of the channel are flexible, on which migrating waves of a sinusoidal nature, having a large wavelength, are superimposed. Cartesian coordinates (*x*, *y*) are utilized, the *y* and *x*-axes are set aside along the normal position and center line, respectively. An external electric field is applied across the EDL in the *x*-axis direction to generate electroosmotic forces. The modified hybrid nanofluid is prepared by mixing 1% volume fraction of solid nanoparticles of *Al₂O₃*, 1% volume proportion of *CuO* and 1% of *Cu* in an aqueous (water) solution.

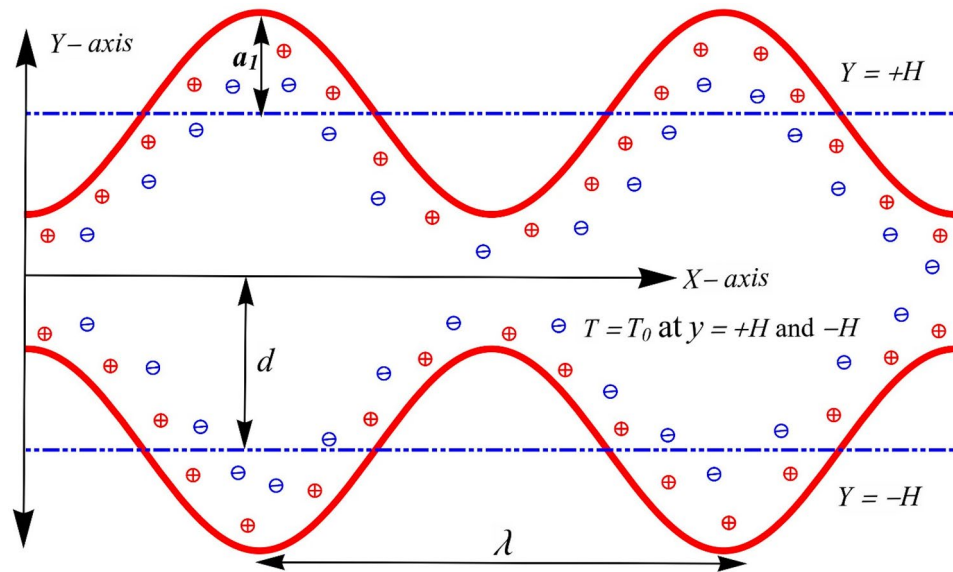


Figure 1. Geometry of the considered problem.

The analysis is conducted in the presence of variable viscosity, magnetic field, viscous dissipation, heterogeneous and homogeneous chemical reactions, and Joule heating. Mathematically, peristaltic walls are given as¹⁸:

$$\pm \bar{H}(\bar{X}, \bar{t}) = \pm a_1 \cos\left(\frac{2\pi}{\lambda}(\bar{X} - c\bar{t})\right) \pm d. \tag{1}$$

where $-\bar{H}(\bar{X}, \bar{t})$ and $+\bar{H}(\bar{X}, \bar{t})$ allocates for the lower and upper walls respectively (see Fig. 1). Further, a simple template for the interaction between a heterogeneous (or surface) reaction and homogeneous (or bulk) reaction in which two chemical species A and B are presumed. A homogeneous reaction can be expressed by cubic autocatalysis, given by the²²:



and that the heterogeneous reaction is²²,



Here α and β are the concentrations of the species A and B, respectively. k_j ($j = s, c$) are the constants rate. It is also supposed that these two reaction processes are single, first-order, isothermal in the catalyst. It is important to note here that these two reactions proceed at the same temperature.

Electro and magnetohydrodynamics. Generalized Ohmic law is given as²⁵:

$$\mathbf{J} = \sigma_{mhf} [\mathbf{E} + \mathbf{V} \times \mathbf{B}]. \tag{4}$$

In this problem $\mathbf{E} = [E_x, 0, 0]$ and $\mathbf{B} = [0, B_0, 0]$. Lorentz force using Eq. (4) is becoming:

$$\mathbf{J} \times \mathbf{B} = [-A_4 \bar{U} B_0^2 \sigma_f, A_4 B_0 \sigma_f E_x, 0]. \tag{5}$$

The Poisson's equation²⁵ for a symmetric channel is characterized as:

$$\nabla^2 \bar{\Omega} = -\frac{\rho_e}{\epsilon}. \tag{6}$$

The net charge density (ρ_e) obeys Boltzmann distribution²⁵ are defined as:

$$\rho_e = ez(\bar{n}_+ - \bar{n}_-), \tag{7}$$

the cations and anions are specified as³³:

$$\bar{n}_{\pm} = \bar{n}_0 e^{\left(\pm \frac{ez}{T_{av} k_B} \bar{\Omega}\right)}. \tag{8}$$

Using Equations. (7) and (8) in (6) and the implementation of the Debye-Hückel approximation³⁴:

$$\frac{d^2\Omega}{dz^2} = \omega^2\Omega, \tag{9}$$

with boundary conditions³³:

$$\begin{aligned} \Omega(y) &= 1, \text{ at } y = 0, \\ \Omega(y) &= 0, \text{ at } y = h. \end{aligned} \tag{10}$$

where ω is an electroosmotic parameter. It is expressed as:

$$\omega = \frac{d}{\lambda_D}, \tag{11}$$

where,

$$\lambda_D = \frac{1}{ez} \left(\frac{\varepsilon K_B T_{av}}{2n_0} \right)^{\frac{1}{2}}. \tag{12}$$

The analytical solution of Eq. (9) subject to boundary conditions (10) takes the resulting form:

$$\Omega(y) = \frac{\sinh(\omega y)}{\sinh(\omega h)}. \tag{13}$$

The governing equations for the current flow configuration are written as^{17,18,21,28}:

$$\frac{\partial \bar{U}}{\partial \bar{X}} + \frac{\partial \bar{V}}{\partial \bar{Y}} = 0, \tag{14}$$

$$\begin{aligned} \rho_{mnf} \left(\bar{U} \frac{\partial \bar{U}}{\partial \bar{X}} + \frac{\partial \bar{U}}{\partial \bar{t}} + \bar{V} \frac{\partial \bar{U}}{\partial \bar{Y}} \right) &= 2 \frac{\partial}{\partial \bar{X}} \left(\mu_{mnf} \frac{\partial \bar{U}}{\partial \bar{X}} \right) + \frac{\partial}{\partial \bar{Y}} \left(\mu_{mnf} \left(\frac{\partial \bar{V}}{\partial \bar{X}} + \frac{\partial \bar{U}}{\partial \bar{Y}} \right) \right) - \frac{\partial \bar{P}}{\partial \bar{X}} \\ &\quad - \rho_e \bar{E}_x + A_4 \sigma_f \bar{U} B_0, \end{aligned} \tag{15}$$

$$\rho_{mnf} \left(\bar{U} \frac{\partial \bar{V}}{\partial \bar{X}} + \bar{V} \frac{\partial \bar{V}}{\partial \bar{Y}} + \frac{\partial \bar{V}}{\partial \bar{t}} \right) = 2 \frac{\partial}{\partial \bar{Y}} \left(\mu_{mnf} \frac{\partial \bar{V}}{\partial \bar{Y}} \right) - \frac{\partial \bar{P}}{\partial \bar{Y}} + \frac{\partial}{\partial \bar{X}} \left(\mu_{mnf} \left(\frac{\partial \bar{V}}{\partial \bar{X}} + \frac{\partial \bar{U}}{\partial \bar{Y}} \right) \right), \tag{16}$$

$$(\rho C)_{mnf} \left(\frac{\partial \bar{T}}{\partial \bar{t}} + \bar{U} \frac{\partial \bar{T}}{\partial \bar{X}} + \bar{V} \frac{\partial \bar{T}}{\partial \bar{Y}} \right) = K_{mnf} \nabla^2 \bar{T} + \Phi + A_4 \sigma_f (\bar{E}_x)^2 + A_4 \sigma_f (\bar{U} B_0)^2 \tag{17}$$

$$\mu_{mnf} \left(\left(\frac{\partial \bar{V}}{\partial \bar{X}} + \frac{\partial \bar{U}}{\partial \bar{Y}} \right)^2 + 2 \left(\frac{\partial \bar{U}}{\partial \bar{X}} \right)^2 + 2 \left(\frac{\partial \bar{V}}{\partial \bar{Y}} \right)^2 \right),$$

$$\frac{d\alpha}{d\bar{t}} = D_A \nabla^2 \alpha - k_c^2 \bar{\alpha} \beta^2, \tag{18}$$

$$\frac{d\beta}{d\bar{t}} = D_B \nabla^2 \beta + k_c^2 \bar{\alpha} \beta^2. \tag{19}$$

In equations, ρ_{mnf} , $\bar{P}(\bar{X}, \bar{Y}, \bar{t})$, \bar{T} , K_{mnf} and Φ represent the modified hybrid nanofluid density, pressure, temperature of nanoliquid, modified hybrid nanoliquid thermal conductivity and heat absorption, respectively (Table 1). For two-phase flows, the thermophysical properties i.e., density, heat capacity, dynamic viscosity, and electric conductivity of modified hybrid nanofluid are given as¹⁴:

$$\begin{aligned} \rho_{mnf} &= (1 - \phi_3) \{ (1 - \phi_2) [(1 - \phi_1) \rho_f + \phi_1 \rho_{p1}] + \phi_2 \rho_{p2} \} + \phi_3 \rho_{p3}, \\ \mu_{mnf} &= \frac{\mu_f}{(1 - \phi_1)^{2.5} (1 - \phi_2)^{2.5} (1 - \phi_3)^{2.5}}, \\ (\rho C_p)_{mnf} &= (1 - \phi_3) \left\{ (1 - \phi_2) \left[\frac{(1 - \phi_1) (\rho C_p)_f}{+ \phi_1 (\rho C_p)_{p1}} \right] + \phi_2 (\rho C_p)_{p2} \right\} + \phi_3 (\rho C_p)_{p3}, \\ \frac{K_{mnf}}{K_{hnf}} &= \frac{K_{p3} + (m - 1) K_{hnf} - (m - 1) \phi_3 (k_{hnf} - k_{p3})}{K_{p3} + (m - 1) K_{hnf} + \phi_3 (k_{hnf} - k_{p3})}, \end{aligned} \tag{20}$$

where

$$\frac{k_{hnf}}{k_{nf}} = \frac{k_{p2} + (m - 1) k_{nf} - (m - 1) \phi_2 (k_{nf} - k_{p3})}{k_{p2} + (m - 1) k_{nf} + \phi_2 (k_{nf} - k_{p3})},$$

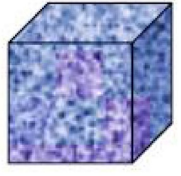
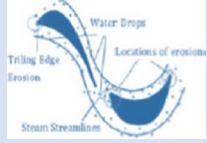
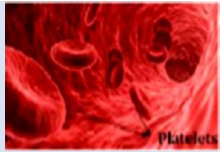
Shapes of nanoparticles	Shape factor (m)	Shape
Bricks	3.7	
Blades	8.6	
Cylinders	4.9	
Platelets	5.7	

Table 1. The shape factor for several types of NPs.

Base fluid/solid particles	ρ (Kg m^3)	C_p (JKg $^{-1}K^{-1}$)	k (Wm $^{-1}K^{-1}$)	σ (Ωm) $^{-1}$
H ₂ O	997.1	4179	0.613	0.05
CuO(ϕ_1)	6500	540	18	6.9×10^{-2}
Cu(ϕ_2)	8933	385	400	59.6×10^6
Al ₂ O ₃ (ϕ_3)	3970	765	40	35×10^6

Table 2. Numerical values of physical properties of base liquid and NPs.

and

$$\frac{k_{nfs}}{k_f} = \frac{k_{p1} + (m - 1)k_f - (m - 1)\phi_1(k_f - k_{p1})}{k_{p3} + (m - 1)k_f + \phi_1(k_f - k_{p1})},$$

$$\frac{\sigma_{mnfs}}{\sigma_{hnfs}} = \frac{\sigma_{p3} + 2\sigma_{hnfs} - 2\phi_3(\sigma_{hnfs} - \sigma_{p3})}{\sigma_{p3} + 2\sigma_{hnfs} + \phi_3(\sigma_{hnfs} - \sigma_{p3})},$$

where

$$\frac{\sigma_{hnfs}}{\sigma_{nfs}} = \frac{\sigma_{p2} + 2\sigma_{nfs} - 2\phi_2(\sigma_{nfs} - \sigma_{p2})}{\sigma_{p2} + 2\sigma_{nfs} + \phi_2(\sigma_{nfs} - \sigma_{p2})},$$

and

$$\frac{\sigma_{nfs}}{\sigma_f} = \frac{\sigma_{p1} + 2\sigma_f - 2\phi_1(\sigma_f - \sigma_{p1})}{\sigma_{p1} + 2\sigma_f + \phi_1(\sigma_f - \sigma_{p1})}.$$

Numerical values of these properties are through Table 2. In Table 1, ϕ_1, ϕ_2, ϕ_3 is volume fractions of CuO, Cu and Al₂O₃ NPs. Subscripts p_1, p_2 and p_3 denoting the CuO, Cu and Al₂O₃ nanoparticles. In addition, m is the shape factor for which numerical values are given in Table 1 for various shape factors.

The transformation between a fixed and movable frame of reference is listed as¹⁸:

$$\begin{aligned} \bar{x} &= \bar{X} - c\bar{t}, \bar{y} = \bar{Y}, \beta = \bar{\beta}, \alpha = \bar{\alpha}, \bar{v}(\bar{x}, \bar{y}) = \bar{V}(\bar{X}, \bar{Y}, \bar{t}), \\ \bar{u}(\bar{x}, \bar{y}) &= \bar{U}(\bar{X}, \bar{Y}, \bar{t}) - c, \bar{p}(\bar{x}, \bar{y}) = \bar{P}(\bar{X}, \bar{Y}, \bar{t}). \end{aligned} \tag{21}$$

Apply conversion to Eqs. (14)-(19), we get

$$\frac{\partial \bar{u}}{\partial \bar{x}} + \frac{\partial \bar{v}}{\partial \bar{y}} = 0, \tag{22}$$

$$\begin{aligned} \rho_{mnf} \left((\bar{u} + c) \frac{\partial \bar{u}}{\partial \bar{x}} + \bar{v} \frac{\partial \bar{u}}{\partial \bar{y}} \right) &= -\frac{\partial \bar{p}}{\partial \bar{x}} + \frac{\partial}{\partial \bar{y}} \left(\mu_{mnf} \frac{\partial \bar{v}}{\partial \bar{y}} \right) + 2 \frac{\partial}{\partial \bar{x}} \left(\mu_{mnf} \left(\frac{\partial \bar{v}}{\partial \bar{x}} + \frac{\partial \bar{u}}{\partial \bar{y}} \right) \right) \\ &- \rho_c \bar{E}_x + A_4 \sigma_f (\bar{u} + c) B_0, \end{aligned} \tag{23}$$

$$\rho_{hnf} \left((\bar{u} + c) \frac{\partial \bar{v}}{\partial \bar{x}} + \bar{v} \frac{\partial \bar{v}}{\partial \bar{y}} \right) = -\frac{\partial \bar{p}}{\partial \bar{y}} + 2 \frac{\partial}{\partial \bar{y}} \left(\mu_{hnf} \frac{\partial \bar{v}}{\partial \bar{y}} \right) + \frac{\partial}{\partial \bar{x}} \left(\mu_{hnf} \left(\frac{\partial \bar{v}}{\partial \bar{x}} + \frac{\partial \bar{u}}{\partial \bar{y}} \right) \right), \tag{24}$$

$$\begin{aligned} (\rho C)_{mnf} \left((\bar{u} + c) \frac{\partial \bar{T}}{\partial \bar{x}} + \bar{v} \frac{\partial \bar{T}}{\partial \bar{y}} \right) &= K_{mnf} \left(\frac{\partial^2 \bar{T}}{\partial \bar{x}^2} + \frac{\partial^2 \bar{T}}{\partial \bar{y}^2} \right) + A_4 \sigma_f (\bar{E}_x)^2 + A_4 \sigma_f B_0^2 (\bar{u} + c)^2 \\ &+ \Phi + \mu_{mnf} \left(\left(\frac{\partial \bar{v}}{\partial \bar{x}} + \frac{\partial \bar{u}}{\partial \bar{y}} \right)^2 + 2 \left(\frac{\partial \bar{u}}{\partial \bar{x}} \right)^2 + 2 \left(\frac{\partial \bar{v}}{\partial \bar{y}} \right)^2 \right), \end{aligned} \tag{25}$$

$$(\bar{u} + c) \frac{\partial \bar{\alpha}}{\partial \bar{x}} + \bar{v} \frac{\partial \bar{\alpha}}{\partial \bar{y}} = D_A \left(\frac{\partial^2 \bar{\alpha}}{\partial \bar{x}^2} + \frac{\partial^2 \bar{\alpha}}{\partial \bar{y}^2} \right) - k_c^2 \bar{\alpha} \bar{\beta}^2, \tag{26}$$

$$(\bar{u} + c) \frac{\partial \bar{\beta}}{\partial \bar{x}} + \bar{v} \frac{\partial \bar{\beta}}{\partial \bar{y}} = D_B \left(\frac{\partial^2 \bar{\beta}}{\partial \bar{x}^2} + \frac{\partial^2 \bar{\beta}}{\partial \bar{y}^2} \right) + k_c^2 \bar{\alpha} \bar{\beta}^2, \tag{27}$$

Reynold’s viscosity model. The Reynolds viscosity model is defined as:

$$\mu_{mnf}(T) = \frac{\mu_0(1 - \alpha_1(T - T_0))}{(1 - \phi_1)^{2.5}(1 - \phi_2)^{2.5}(1 - \phi_3)^{2.5}}. \tag{28}$$

Using the subsequent dimensionless quantities:

$$\begin{aligned} x &= \frac{\bar{x}}{\lambda}, y = \frac{\bar{y}}{d}, \theta = \frac{T - T_0}{T_0}, u = \frac{\bar{u}}{c}, Ec = \frac{c^2}{C_f T_0}, v = \frac{\bar{v}}{c\delta}, h = \frac{\bar{H}}{d}, a = \frac{a_1}{d}, p = \frac{d^2 \bar{p}}{c\lambda\mu_0}, \\ Pr &= \frac{\mu_0 C_f}{K_f}, Br = Pr E, \varepsilon = \frac{d^2 \Phi}{T_0 k_f}, M = \sqrt{\frac{\sigma_f}{\mu_0} B_0 d}, Gr = \frac{\rho_f \beta_f g T_0 d^2}{\mu_0 c}, u = \frac{\partial \psi}{\partial y}, \\ U_{hs} &= -\frac{\varepsilon \bar{E}_x}{\mu_0}, S = \frac{d^2 \sigma_f \bar{E}_x^2}{k_f T_0}, \bar{\alpha} = \frac{f}{\alpha_0}, \bar{\beta} = \frac{g}{\alpha_0}, K = \frac{k_c d^2 \alpha_0^2}{\nu}, K_s = \frac{k_c d}{D_A}, Sc = \frac{\nu}{D_B}, \\ v &= \frac{\mu_0}{\rho_0}, \phi = \frac{C - C_0}{C_0}, \xi = \frac{D_B}{D_A}, \nu = -\frac{\partial \psi}{\partial x}. \end{aligned} \tag{29}$$

Utilizing “long wavelength and low Reynolds number approximations”, Eqs. (22)-(27) have following form:

$$\frac{\partial p}{\partial x} = A_1 \frac{\partial}{\partial y} \left[(1 - \alpha\theta) \frac{\partial^2 \psi}{\partial y^2} \right] + U_{hs} \Omega''(y) - A_4 M^2 \left(\frac{\partial \psi}{\partial y} + 1 \right) = 0, \tag{30}$$

$$\frac{\partial p}{\partial y} = 0, \tag{31}$$

$$A_3 \frac{\partial^2 \theta}{\partial y^2} + A_1 Br (1 - \alpha\theta) \left(\frac{\partial^2 \psi}{\partial y^2} \right)^2 + A_4 Br M^2 \left(\frac{\partial \psi}{\partial y} + 1 \right)^2 + A_4 S + \varepsilon = 0, \tag{32}$$

$$\frac{1}{Sc} \frac{\partial^2 f}{\partial y^2} - K_f g^2 = 0, \tag{33}$$

$$\frac{\xi}{Sc} \frac{\partial^2 g}{\partial y^2} + Kfg^2 = 0. \quad (34)$$

A_1 , A_3 , and A_4 are defined as:

$$A_1 = \frac{1}{(1 - \phi_1)^{2.5} (1 - \phi_2)^{2.5} (1 - \phi_3)^{2.5}},$$

$$A_3 = \frac{k_{mnf}}{k_f} = \frac{k_{s_3} + (m - 1)k_{hnf} - (m - 1)\phi_3(k_{hnf} - k_{s_3})}{k_{s_3} + (m - 1)k_{hnf} + \phi_3(k_{hnf} - k_{s_3})} \times \frac{k_{s_2} + (m - 1)k_{nf} - (m - 1)\phi_2(k_{nf} - k_{s_3})}{k_{s_2} + (m - 1)k_{nf} + \phi_2(k_{nf} - k_{s_3})}$$

$$\times \frac{k_{s_2} + (m - 1)k_{nf} - (m - 1)\phi_2(k_{nf} - k_{s_3})}{k_{s_2} + (m - 1)k_{nf} + \phi_2(k_{nf} - k_{s_3})}, \quad (35)$$

and

$$A_4 = \frac{\sigma_{mnf}}{\sigma_f} = \frac{\sigma_{s_3} + 2\sigma_{hnf} - 2\phi_3(\sigma_{hnf} - \sigma_{s_3})}{\sigma_{s_3} + 2\sigma_{hnf} + \phi_3(\sigma_{hnf} - \sigma_{s_3})} \times \frac{\sigma_{s_2} + 2\sigma_{nf} - 2\phi_2(\sigma_{nf} - \sigma_{s_2})}{\sigma_{s_2} + 2\sigma_{nf} + \phi_2(\sigma_{nf} - \sigma_{s_2})}$$

$$\times \frac{\sigma_{s_1} - 2\phi_1(\sigma_f - \sigma_{s_1}) + 2\sigma_f}{\sigma_{s_1} + \phi_1(\sigma_f - \sigma_{s_1}) + 2\sigma_f}.$$

The dimensionless boundary conditions are listed as³⁴:

$$\psi = 0, \quad \frac{\partial^2 \psi}{\partial y^2} = 0, \quad \frac{\partial \theta}{\partial y} = 0, \quad \text{at } y = 0,$$

$$\psi = F, \quad \frac{\partial \psi}{\partial y} = -1, \quad \theta = 0, \quad \text{at } y = h. \quad (36)$$

$$f = 1, \quad g = 0, \quad \text{at } y = 0,$$

$$\frac{\partial f}{\partial y} - K_s f = 0, \quad \xi \frac{\partial g}{\partial y} + K_s g = 0, \quad \text{at } y = h.$$

The diffusion coefficients of chemical compounds B and A are not same in general. We can consider them equal in size as a particular case, and thus $D_A = D_B$. Then Eqs. (33) and (34) result in the following relationship²¹:

$$f + g = 1. \quad (37)$$

Hence

$$\frac{1}{Sc} \frac{\partial^2 f}{\partial y^2} - Kf(1 - f)^2 = 0, \quad (38)$$

and relevant boundary conditions turn into

$$f = 1, \quad \text{at } y = 0, \quad (39)$$

$$\frac{\partial f}{\partial y} = K_s f, \quad \text{at } y = h.$$

Moreover, upon removal of pressure among Eqs. (30) and (31):

$$0 = A_1 \frac{\partial^2}{\partial y^2} \left[(1 - \alpha\theta) \frac{\partial^2 \psi}{\partial y^2} \right] + U_{hs} \Omega'''(y) - A_4 M^2 \frac{\partial^2 \psi}{\partial y^2} = 0. \quad (40)$$

Solution methodology. The deemed Homotopy equation for the differential system has the following form:

$$H(\psi, p) = (1 - p)[L_1(\psi) - L_1(\psi_0)] + p \left[\begin{array}{l} A_1 \frac{\partial^2}{\partial y^2} \left\{ (1 - \alpha\theta) \frac{\partial^2 \psi}{\partial y^2} \right\} + \\ U_{hs} \Omega'''(y) - A_4 M^2 \frac{\partial^2 \psi}{\partial y^2} \end{array} \right], \quad (41)$$

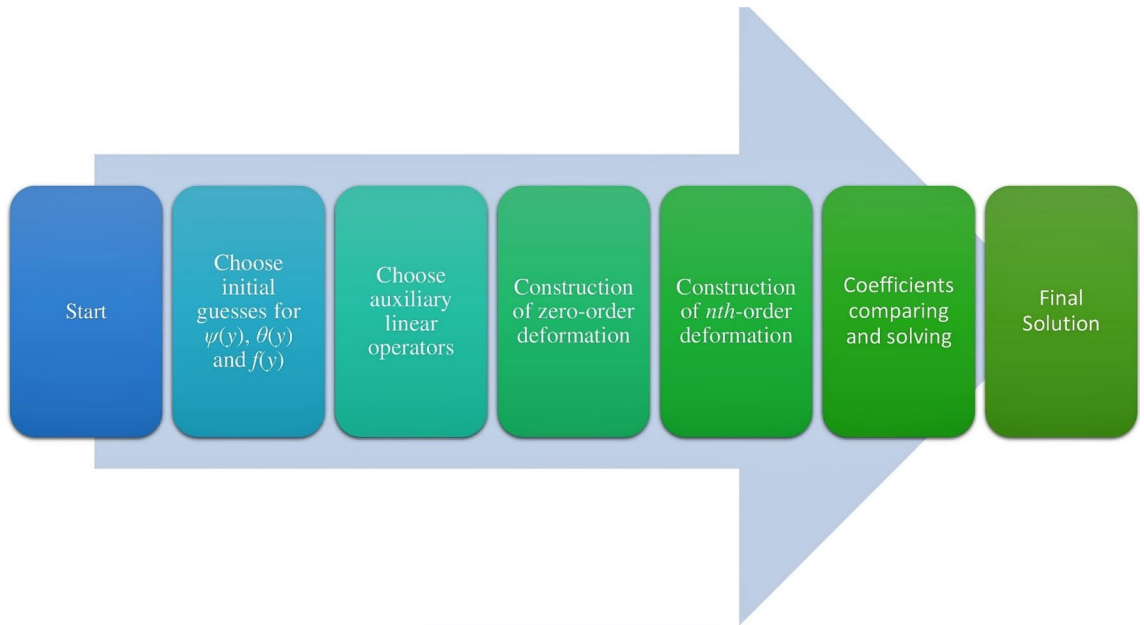


Figure 2. Flow chart of HPM.

$$H(\theta, p) = (1 - p)[L_2(\theta) - L_2(\theta_0)] + p \left[A_3 \frac{\partial^2 \theta}{\partial y^2} + A_1 Br(1 - \alpha\theta) \left(\frac{\partial^2 \psi}{\partial y^2} \right)^2 + A_4 BrM^2 \left(\frac{\partial \psi}{\partial y} + 1 \right)^2 + A_4 S + \varepsilon \right], \tag{42}$$

$$H(\phi, p) = (1 - p)[L_3(\phi) - L_3(\phi_0)] + p \left[\frac{1}{Sc} \frac{\partial^2 f}{\partial y^2} - Kf(1 - f)^2 \right]. \tag{43}$$

Relevant linear operators are received as:

$$L_1 = A_1 \frac{\partial^4}{\partial y^4}, \tag{44}$$

$$L_2 = A_3 \frac{\partial^2}{\partial y^2}, \tag{45}$$

$$L_3 = \frac{\partial^2}{\partial y^2}. \tag{46}$$

Initial guesses are described as:

$$\psi_0 = \frac{3Fh^2y + h^3y - Fy^3 - hy^3}{2h^3}, \tag{47}$$

$$\theta_0 = 0, \tag{48}$$

$$f_0 = \frac{1 - hL + Ly}{1 - hL}. \tag{49}$$

The series extension is expressed as:

$$\begin{aligned} \psi(y, p) &= \psi_0 + p\psi_1 + p^2\psi_2 + \dots, \\ \theta(y, p) &= \theta_0 + p\theta_1 + p^2\theta_2 + \dots, \\ f(y, p) &= f_0 + pf_1 + p^2f_2 + \dots. \end{aligned} \tag{50}$$

The second, first and zeroth order systems of differential equations are achieved and then resolved with the assistance of Mathematica software. The HPM process is presented as a step-by-step diagram in Fig. 2.

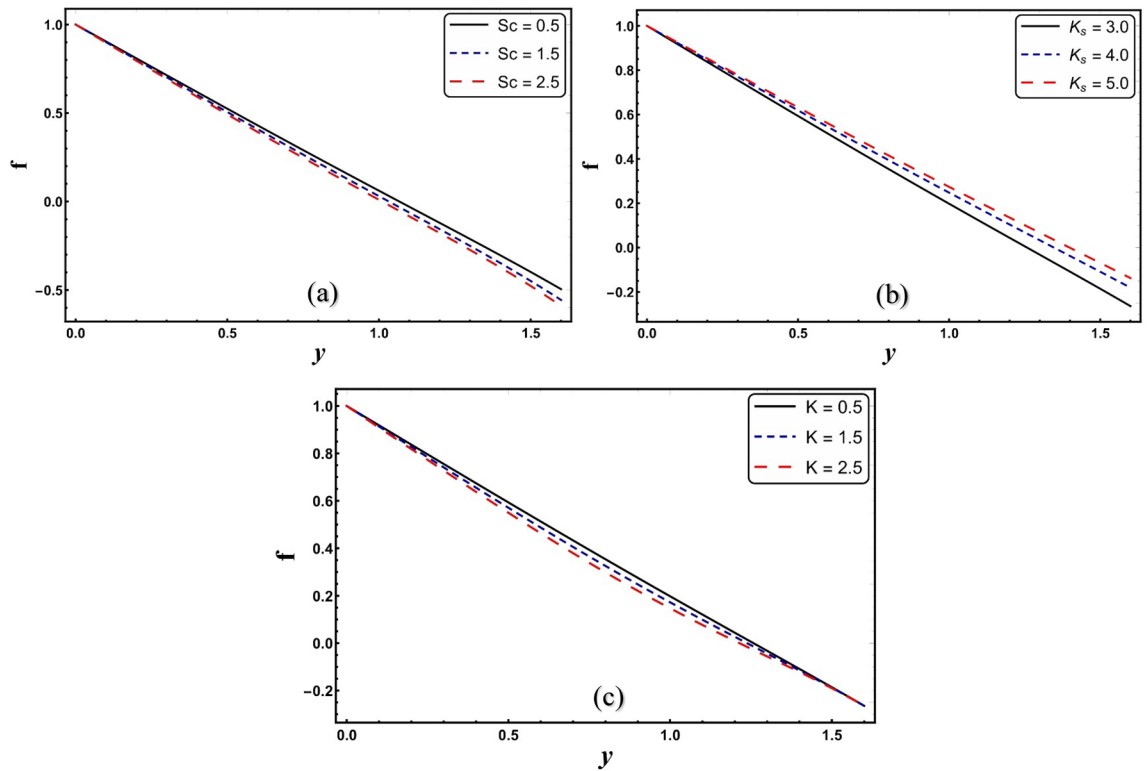


Figure 3. (a–c) Velocity profile for change in different embedded parameters.

Zeroth order system.

$$A_1 \psi_0^{(4)} [y] = 0,$$

$$A_3 \theta_0'' [y] = 0,$$

$$f_0'' [y] = 0.$$

First order system.

$$US\omega^3 \cosh [y\omega] \text{Csch}[h\omega] - A_4 M^2 \psi_0'' [y] - A_1 \alpha \theta_0'' [y] \psi_0'' [y] - 2A_1 \alpha \theta_0' [y] \psi_0^{(3)} [y] - A_1 \alpha \theta_0 [y] \psi_0^{(4)} [y] + A_1 \psi_1^{(4)} [y] = 0,$$

$$A_4 S + \varepsilon + A_4 Br M^2 (1 + \psi_0' [y])^2 + A_3 \theta_1'' [y] + A_1 Br (1 - \alpha \theta_0 [y]) \psi_0'' [y]^2 = 0,$$

$$-Kf_0 [y] + 2Kf_0 [y]^2 - Kf_0 [y]^3 - f_0'' [y] + \frac{f_0'' [y]}{Sc} + f_1'' [y] = 0.$$

Similarly, the second order system is achieved. Solutions for the above systems are analyzed using graphs and tables in the next section.

Results and discussion

In this part, the impact of several relevant parameters in flow and heat transfer performance of a modified hybrid nanofluid flow through a symmetrical channel is analytically analyzed in detail.

Concentration profile. Figures 3a–c display the results of concentration profile for change in Sc , K_s , and K . Figure 3a reveals that concentration profile decreases for higher Sc . Since the Schmidt number characterizes the flow of a liquid in which various processes of mass diffusion and momentum diffusion occur. This trend is in accordance with the Alarabi et al.²². Thus, higher Sc values reduce the rate of mass diffusion, which leads to the particles to scatter and thus a decrease in concentration is seen. It is observed from Fig. 3b that concentration enhances for larger values of heterogeneous reaction parameter. On the other hand, with a change in K , the reverse behavior in concentration is observed, as shown in Fig. 3c.

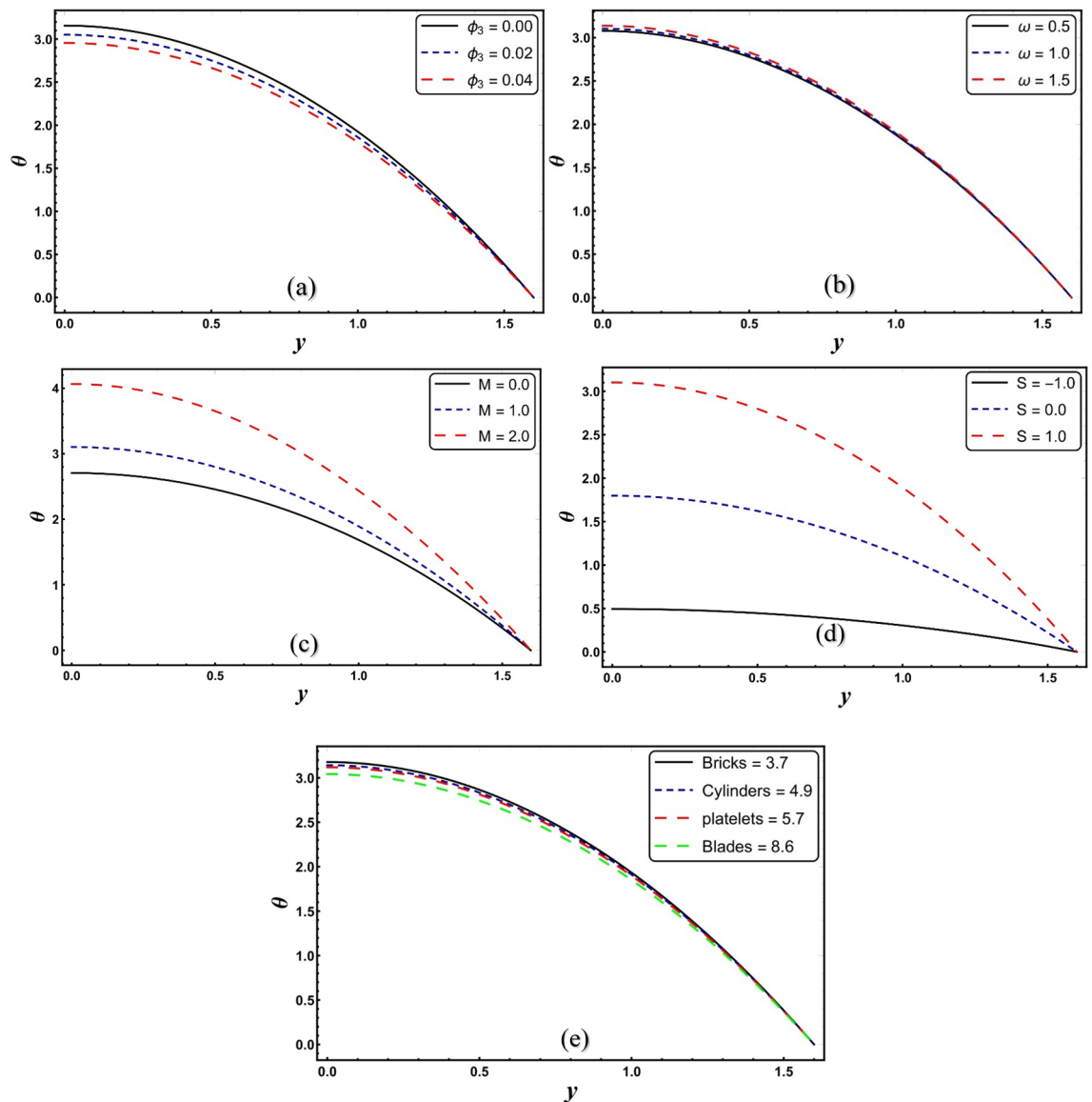


Figure 4. (a–e) θ for change in various parameters.

Temperature profile. This subsection investigates the temperature of nanofluid containing modified hybrid nanoparticles (see Figs. 4a–e). Figure 4a predicts that the temperature curve of modified nanofluid decreases for a higher ϕ_3 . The addition of nanomaterials to the working liquid increases the heat transmission capability of the material. This leads to a reduction in temperature. Thus, the modified model is of immense significance to the mechanism of mechanical devices in which cooling agents are utilized. This finding is compatible with the Abbasi et al.¹⁴ Figure 4b demonstrates that temperature of modified nanofluid significantly elevates with incremental parameter ω . It is well understood that the electroosmotic force is a flow-resisting force that increases collisions between liquid particles. The internal kinetic energy of moving particles in a direction of flow increases as the frequency of collisions increases, resulting in an increase in temperature. Figure 4c shows that increasing S causes a significant increase in temperature of the modified nanofluid. Physically, this is due to the conversion of dissipated electrical energy into thermal energy. Similar trend is also encountered for higher M (see Fig. 4d). The geometry impact phenomena of nanomaterials are exemplified for various shapes, and this is reflected that varying the values of m give impact to various forms of NPs in the temperature field (see Fig. 4e). It is seen that brick-shaped NPs produce more heat than other NPs shapes. Brick-shaped NPs predominate compared to cylinder and plate-shaped NPs, while blade-shaped NPs give the minimum temperature.

Heat transfer rate at the wall. Tables 3 is made to see the behavior of heat transfer rate at the wall $\left(-\frac{k_{mnf}}{k_f}\theta'(h)\right)$ for various values of the governing parameters. Table 3 first column illustrates increased $-\frac{k_{mnf}}{k_f}\theta'(h)$ with growth in nanoparticles volume fraction that is consistent with Akbar et al.¹⁸ The second column of Table 3 indicates that ω upsurges the $-\frac{k_{mnf}}{k_f}\theta'(h)$ when it is installed in such a way that peristaltic pumping is assisted.

Parameters	Different shapes of nanoparticles						
	ω	S	M	Bricks	Cylinders	Platelets	Blades
0.01	1.0	1.0	1.0	4.0852	4.0853	4.0854	4.0858
0.02				4.1581	4.1584	4.1586	4.1593
0.04				4.3090	4.3096	4.3100	4.3111
	0.5			4.0797	4.0799	4.0800	4.0804
	1.0			4.0852	4.0853	4.0854	4.0858
	1.5			40,929	40,930	40,932	40,935
		-1.0		0.7008	0.7009	0.7009	0.7010
		0.0		2.3930	2.3931	2.3932	2.3934
		1.0		4.0852	4.0853	4.0854	4.0858
			0.0	3.6855	3.6857	3.6858	3.6861
			1.0	4.0852	4.0853	4.0854	4.0858
			2.0	5.1678	5.1680	5.1681	5.1686

Table 3. Numerical values of $\left(-\frac{k_{mnf}}{k_f}\theta'(h)\right)$ against different involved parameters.

M	Base fluid (H_2O) ($\phi_1 = \phi_2 = \phi_3 = 0$)	Nanofluid ($Al_2O_3-H_2O$) ($\phi_1 = 0, \phi_2 = 0, \phi_3 = 0.03$)	Hybrid nanofluid ($Cu + Al_2O_3-H_2O$) ($\phi_1 = 0.015, \phi_3 = 0.015, \phi_2 = 0$)	Modified hybrid nanofluid ($CuO + Cu + Al_2O_3-H_2O$) ($\phi_1 = 0.01, \phi_2 = 0.01, \phi_3 = 0.01$)
0.0	3.55898	3.58731	3.66059	3.68559
1.0	3.93591	3.96423	4.05441	4.08521
2.0	4.95542	4.99189	5.12308	5.1678

Table 4. Comparison of $\left(-\frac{k_{mnf}}{k_f}\theta'(h)\right)$ for regular base fluid, ordinary nanofluid, hybrid nanofluid and modified hybrid nanofluid.

Analogous behavior is noted for S (see third column). The fourth column shows that the $-\frac{k_{mnf}}{k_f}\theta'(h)$ is increased by improving M . When a magnetic field is applied, the temperature of the modified hybrid nanofluid increases, thereby improving the heat transfer phenomenon at the wall. $-\frac{k_{mnf}}{k_f}\theta'(h)$ is greater in blade-shaped NPs compared to other shaped NPs. Blade-shaped NPs are used to maintain heat transfer in technical systems.

Comparison of heat transfer rate. Table 4 highlights the impact of base fluid (H_2O), ordinary nanofluid ($Al_2O_3-H_2O$), hybrid nanofluid ($Cu + Al_2O_3-H_2O$) and modified hybrid nanofluid ($CuO + Cu + Al_2O_3-H_2O$) on heat transfer rate. It is concluded that water with modified hybrid nanoparticles has higher heat transfer rate as compared to base fluid (H_2O), ordinary nanofluid ($Al_2O_3-H_2O$), hybrid nanofluid ($Cu + Al_2O_3-H_2O$). This is due to increased thermal conductivity of the modified hybrid nanofluids.

Isotherms. The temperature distribution in the flow field is reflected by isotherms. Isotherms lines of modified hybrid nanofluid under the effects of M and S are drawn through Figs. 5,6. Figure 5a,b show that increasing M causes a notable change in the isotherms. It appears from Fig. 6A,B that the trapped bolus rises by increasing S .

Velocity profile. Figure 7a–e are plotted to explore the response of velocity of ($Cu + CuO + Al_2O_3$) modified hybrid nanofluid against different involved parameters. Viewed from Fig. 7a that the magnitude of velocity of modified nanofluid reduces with increased NPs volume fraction. This is due to a higher volume fraction of aluminum oxide NPs (ϕ_3), which increases the viscosity of the liquid, and therefore resists the movement of the liquid. This outcome is in accordance with Abbasi et al.¹⁷ Figure 7b illustrates that velocity grows with rising values of α . This means that the modified nanofluid, whose viscosity depends on temperature, reflects a higher velocity near the middle of the channel compared to the velocity of the nanofluid, which has a constant viscosity ($\alpha = 0$). Figure 7c shows that increasing the electroosmotic parameter boosts nanofluid flow. The phenomenon of ELD affects an electroosmotic parameter. Velocity declines for larger ω when $U_{hs} = -1.0$. Figure 7d outlines that nanofluid flow is reduced by strengthening U_{hs} . For auxiliary electric field velocity is higher and lower for the opposing electric field. U_{hs} is reliant on the electric field, which governs the flow in this case. The applied electric field has a direct relationship with U_{hs} . Thus, at the positive value of U_{hs} it acts as a hindering force in the momentum equation, and at negative values it maintains the fluid flow. A similar behavior on velocity is also seen for higher Hartman number (see Fig. 7e). A Lorentz force is created in the flow when the Hartmann number (M) is increased, which causes the velocity to reduce.

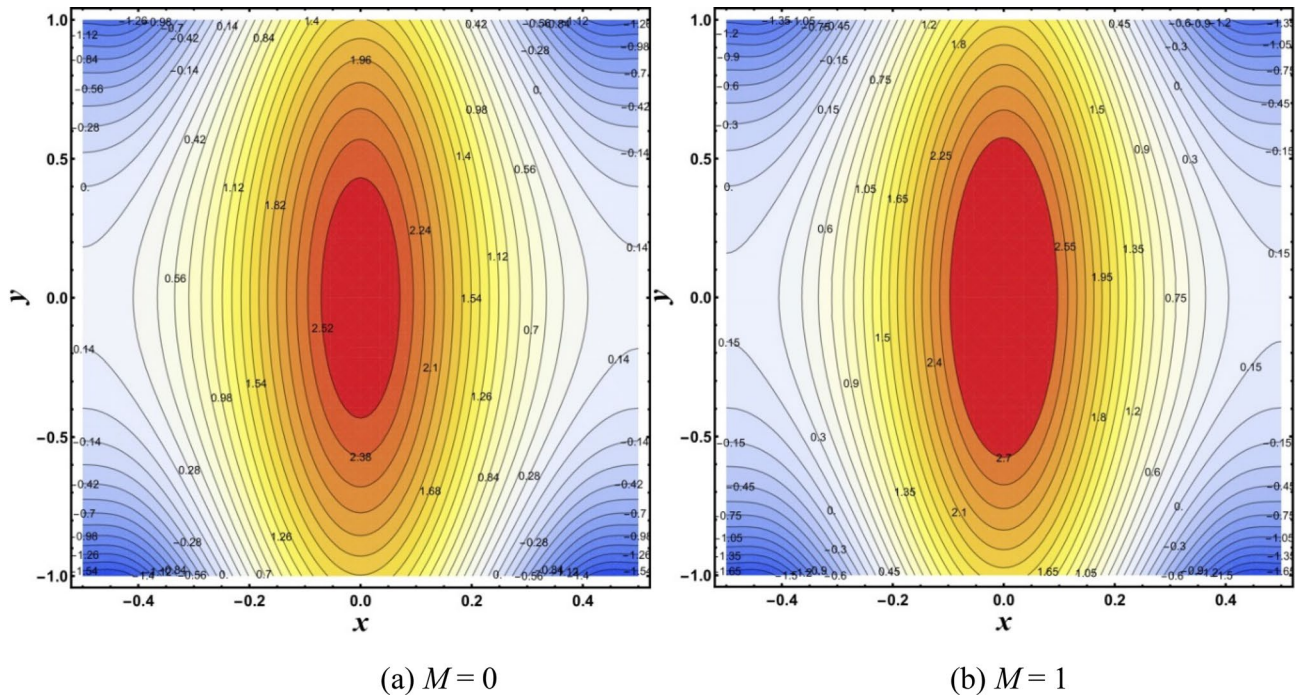


Figure 5. Isotherms for change in M .

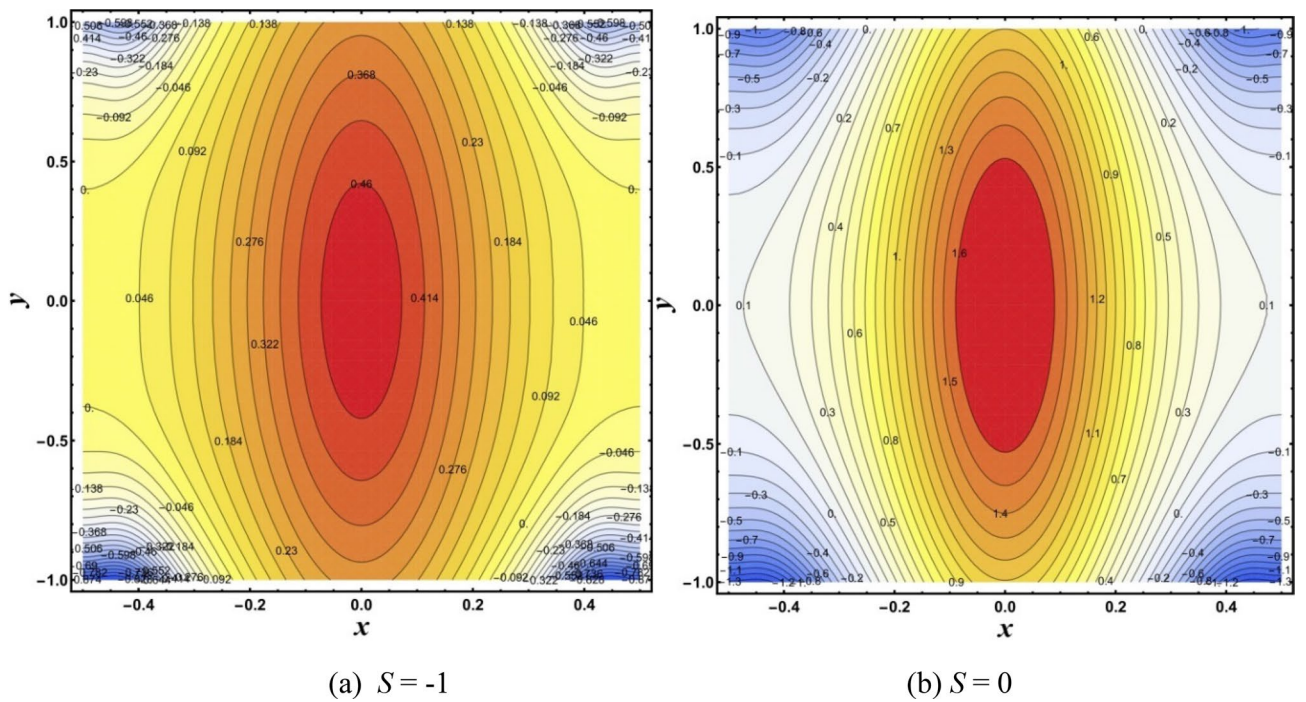
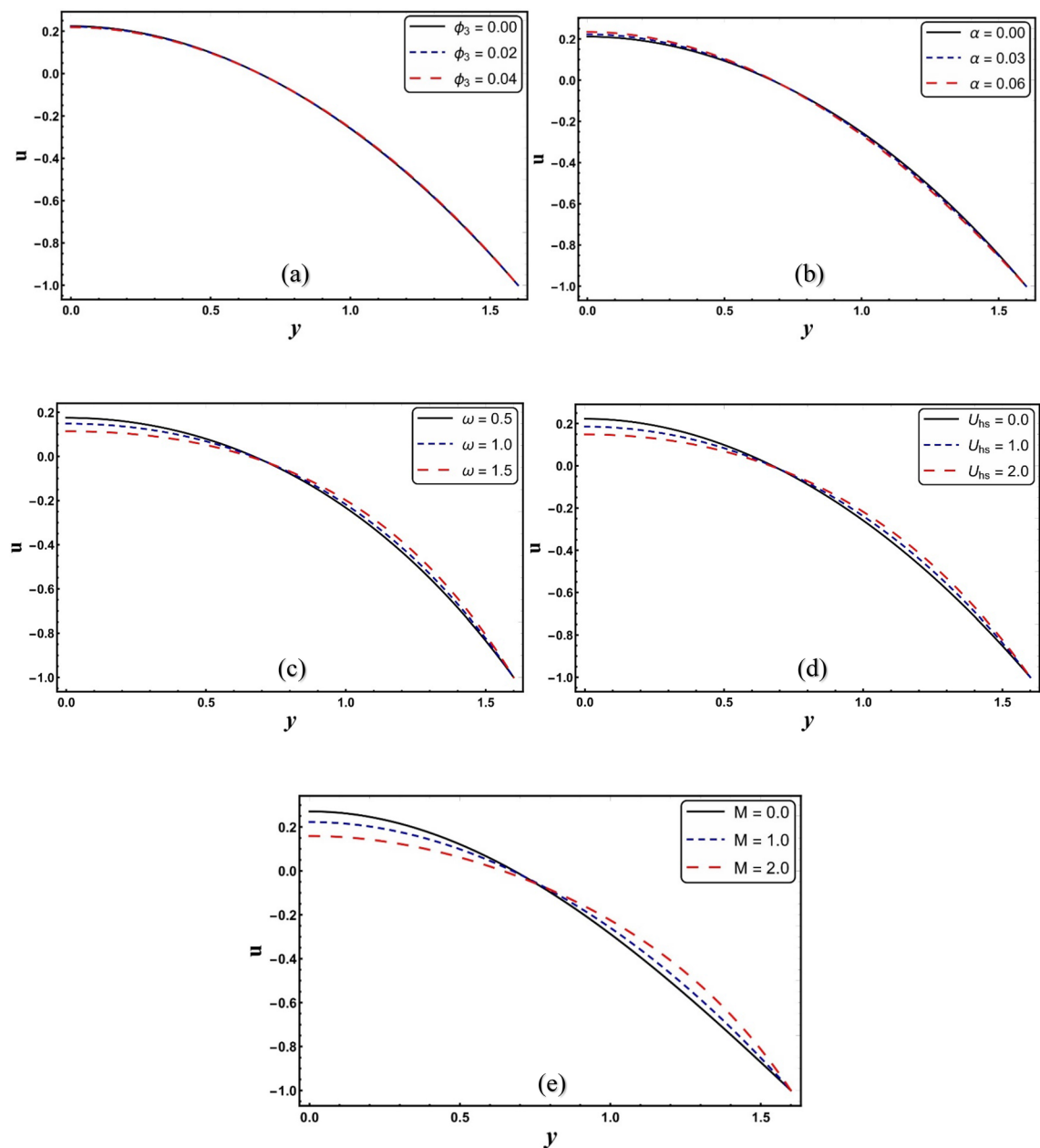


Figure 6. Isotherms for change in S .

Pressure gradient. Figure 8a–e are made to evaluate the change in pressure gradient with respect to x across various embedded parameters. Figure 8a shows a reduction in pressure gradient with increasing concentration of nanomaterials. The addition of nanomaterials increases the resistance to fluid flow and thus reduces the pressure gradient. A reverse trend is seen in Fig. 8b with the impact of viscosity parameter. From Fig. 8c, pressure gradient decreases by improving electroosmotic parameter. The existence of EDL in charged surfaces abstains the flow, therefore pressure gradient decreases. Figure 8d portrays that pressure gradient develops by improving U_{fs} . The pressure gradient is suppressed by increasing M (see Fig. 8e). The pressure gradient change to increase the Hartmann number is large when $M > 1$.

Figure 7(a-e): Velocity profile for change in M .**Figure 7.** (a–e) Velocity profile for change in M .

A comparison between analytically (HPM) and numerical results (NDSolve) are also presented via Fig. 9. It is seen that both outcomes are consistent.

Conclusions

The present endeavor brings out the collective effects of electro-magneto hydrodynamic, temperature dependent viscosity, homogeneous and heterogeneous chemical reaction rates in the peristaltic movement of a modified hybrid nanofluid containing Al_2O_3 , CuO , Cu NPs in an aqueous solution. Significant observations are enumerated below:

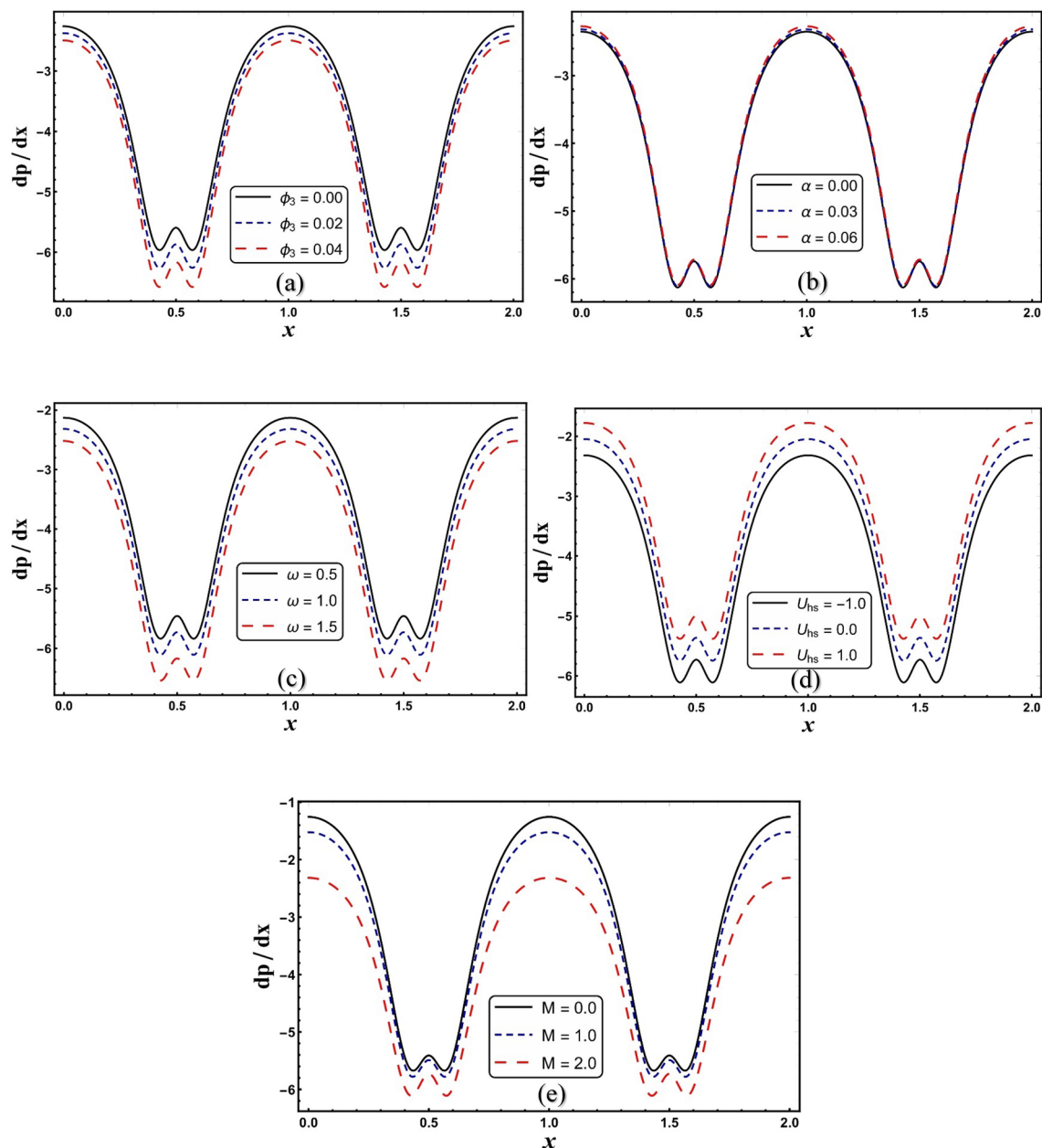


Figure 8. (a–e) Pressure gradient for change in M .

- Heterogeneous reaction parameter aids for enhancing the concentration profiles while the homogeneous reaction parameter reduces the concentration.
- Temperature of modified HNFs significantly elevates with an increment in electroosmotic parameter.
- Rate of heat-transfer at the boundary is greater for blade-shaped NPs compared to other shaped NPs.
- Modified hybrid nanofluid has superior heat transfer rate relative to base fluid (H_2O), ordinary nanofluid ($Al_2O_3-H_2O$), hybrid nanofluid ($Cu + Al_2O_3-H_2O$).
- The isotherms show a notable change when the Hartman number is increased.
- A development in pressure gradient is obtained by improving the Helmholtz-Smoluchowski velocity.

The results of this theoretical study can be extended by discussing it for various other Newtonian nanofluids through straight and curved channels. In addition, considering slippage conditions at the boundaries gives this study an accurate picture of reality.

Data availability

The datasets used and analyzed during the current study available from the corresponding author on reasonable request.

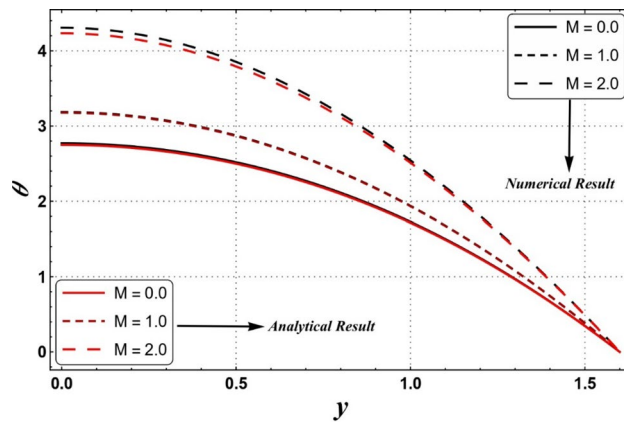


Figure 9. A comparison of the results obtained at analytical technique (HPM) and numerical technique (NDSolve).

Received: 9 May 2022; Accepted: 26 July 2022

Published online: 12 August 2022

References

- Choi, S. U. & Eastman, J. A. (1995). Enhancing thermal conductivity of fluids with nanoparticles (No. ANL/MSD/CP-84938; CONF-951135-29). Argonne National Lab., IL (United States).
- Eastman, J. A., Choi, U. S., Li, S., Thompson, L. J. & Lee, S. Enhanced thermal conductivity through the development of nanofluids. *MRS Online Proc. Lib. (OPL)* **457**, 1 (1996).
- Xuan, Y. & Li, Q. Heat transfer enhancement of nanofluids. *Int. J. Heat Fluid Flow* **21**(1), 58–64 (2000).
- Mohanty, P. & Ram, S. Dissolution of Eu_3^+ cations in mesopores in amorphous Al_2O_3 and controlled reconstructive nucleation and growth of $\gamma\text{-Al}_2\text{O}_3$ nanoparticles. *J. Eur. Ceram. Soc.* **22**(6), 933–945 (2002).
- Mondragón, R., Segarra, C., Martínez-Cuenca, R., Juliá, J. E. & Jarque, J. C. Experimental characterization and modeling of thermophysical properties of nanofluids at high temperature conditions for heat transfer applications. *Powder Technol.* **249**, 516–529 (2013).
- Buongiorno, J. Convective transport in nanofluids (2006).
- Tiwari, R. K. & Das, M. K. Heat transfer augmentation in a two-sided lid-driven differentially heated square cavity utilizing nanofluids. *Int. J. Heat Mass Transf.* **50**(9–10), 2002–2018 (2007).
- Lazarus, G. Nanofluid heat transfer and applications. *J. Therm. Eng.* **1**(2), 113–115 (2015).
- Abbasi, A. & Farooq, W. A numerical simulation for transport of hybrid nanofluid. *Arab. J. Sci. Eng.* **45**(11), 9249–9265 (2020).
- Ali, K. *et al.* Quasi-linearization analysis for heat and mass transfer of magnetically driven 3rd-grade (Cu-TiO₂/engine oil) nanofluid via a convectively heated surface. *Int. Commun. Heat Mass Transfer* **135**, 106060 (2022).
- Jamshed, W. *et al.* Physical specifications of MHD mixed convective of Ostwald-de Waele nanofluids in a vented-cavity with inner elliptic cylinder. *Int. Commun. Heat Mass Transfer* **134**, 106038 (2022).
- Jamshed, W. *et al.* Entropy amplified solitary phase relative probe on engine oil-based hybrid nanofluid. *Chin. J. Phys.* **77**, 1654–1681 (2022).
- Jamshed, W. *et al.* Thermal efficiency enhancement of solar aircraft by utilizing unsteady hybrid nanofluid: A single-phase optimized entropy analysis. *Sustain. Energy Technol. Assess.* **52**, 101898 (2022).
- Abbasi, A. *et al.* Optimized analysis and enhanced thermal efficiency of modified hybrid nanofluid (Al_2O_3 , CuO, Cu) with nonlinear thermal radiation and shape features. *Case Stud. Therm. Eng.* **28**, 101425 (2021).
- Shapiro, A. H., Jaffrin, M. Y. & Weinberg, S. L. Peristaltic pumping with long wavelengths at low Reynolds number. *J. Fluid Mech.* **37**(4), 799–825 (1969).
- Akram, S., Nadeem, S., Ghafoor, A. & Lee, C. Consequences of nanofluid on peristaltic flow in an asymmetric channel. *Int. J. Basic Appl. Sci. IJBAS-IJENS* **12**(5), 75–96 (2012).
- Abbasi, F. M., Shanakhat, I. & Shehzad, S. A. Analysis of entropy generation in peristaltic nanofluid flow with Ohmic heating and Hall current. *Phys. Scr.* **94**(2), 025001 (2019).
- Akbar, Y., Abbasi, F. M. & Shehzad, S. A. Thermal radiation and Hall effects in mixed convective peristaltic transport of nanofluid with entropy generation. *Appl. Nanosci.* **10**(12), 5421–5433 (2020).
- Reddy, S. R. R., Basha, H. T. & Duraisamy, P. Entropy generation for peristaltic flow of gold-blood nanofluid driven by electrokinetic force in a microchannel. *Eur. Phys. J. Spec. Top.* **1**, 1–15 (2022).
- Ravikiran, G., & Radhakrishnamacharya, G. Effect of homogeneous and heterogeneous chemical reactions on peristaltic transport of a Jeffrey fluid through a porous medium with slip condition (2015).
- Tanveer, A., Hayat, T., Alsaedi, A. & Ahmad, B. Mixed convective peristaltic flow of Sisko fluid in curved channel with homogeneous-heterogeneous reaction effects. *J. Mol. Liq.* **233**, 131–138 (2017).
- Alarabi, T. H., Rashad, A. M. & Mahdy, A. Homogeneous-heterogeneous chemical reactions of radiation hybrid nanofluid flow on a cylinder with joule heating: Nanoparticles shape impact. *Coatings* **11**(12), 1490 (2021).
- Khan, N. S., Humphries, U. W., Kumam, W., Kumam, P., & Muhammad, T. Bioconvection Casson nanofluid film sprayed on a stretching cylinder in the portfolio of homogeneous-heterogeneous chemical reactions. *ZAMM-J. Appl. Math. Mech./Zeitschrift für Angewandte Mathematik und Mechanik*, e202000222 (2022).
- Rice, C. L. & Whitehead, R. Electrokinetic flow in a narrow cylindrical capillary. *J. Phys. Chem.* **69**(11), 4017–4024 (1965).
- Tang, G. H., Li, X. F., He, Y. L. & Tao, W. Q. Electroosmotic flow of non-Newtonian fluid in microchannels. *J. Nonnewton. Fluid Mech.* **157**(1–2), 133–137 (2009).
- Prakash, J., Sharma, A. & Tripathi, D. Thermal radiation effects on electroosmosis modulated peristaltic transport of ionic nanofluids in biomicrofluidics channel. *J. Mol. Liq.* **249**, 843–855 (2018).
- Sharma, A., Tripathi, D., Sharma, R. K. & Tiwari, A. K. Analysis of double diffusive convection in electroosmosis regulated peristaltic transport of nanofluids. *Physica A* **535**, 122148 (2019).

28. Akram, J., Akbar, N. S. & Maraj, E. N. A comparative study on the role of nanoparticle dispersion in electroosmosis regulated peristaltic flow of water. *Alex. Eng. J.* **59**(2), 943–956 (2020).
29. Sridhar, V. & Ramesh, K. Peristaltic activity of thermally radiative magneto-nanofluid with electroosmosis and entropy analysis. *Heat Transfer* **51**(2), 1668–1690 (2022).
30. Abbasi, A., Mabood, F., Farooq, W. & Khan, S. U. Radiation and joule heating effects on electroosmosis-modulated peristaltic flow of Prandtl nanofluid via tapered channel. *Int. Commun. Heat Mass Transfer* **123**, 105183 (2021).
31. Abbasi, A., Farooq, W., Khan, S. U., Amer, H. & Khan, M. I. Electroosmosis optimized thermal model for peristaltic flow of with Sutterby nanoparticles in asymmetric trapped channel. *Eur. Phys. J. Plus* **136**(12), 1–18 (2021).
32. Kotnurkar, A. S. & Talawar, V. T. Impact of electroosmosis and joule heating effects on peristaltic transport with thermal radiation of hyperbolic tangent fluid through a porous media in an endoscope. *Part. Differ. Equ. Appl. Math.* **5**, 100340 (2022).
33. Akbar, Y., Alotaibi, H., Javed, U., Naz, M., & M. Alam, M. Electroosmosis modulated peristaltic transport of Carreau magneto-nanofluid with modified Darcy's law. *Waves in Random and Complex Media*, 1–21 (2022).
34. Akbar, Y. & Alotaibi, H. Electroosmosis-optimized thermal model for peristaltic transportation of thermally radiative magnetized liquid with nonlinear convection. *Entropy* **24**(4), 530 (2022).

Acknowledgements

Jun Wang was supported by NNSF of China (Grant 11971202), and Outstanding Young foundation of Jiangsu Province No. BK20200042.

Author contributions

Y.A.: Supervision, Conceptualization, Formal analysis, Writing—original draft, Writing—review & editing. A.H.: Data curation, Investigation, Methodology, Writing—original draft, Writing—review & editing. J.W.: Software, Formal analysis, Writing—review & editing. R.S.: Data curation, Methodology, funding, Writing—review & editing.

Competing interests

The authors declare no competing interests.

Additional information

Correspondence and requests for materials should be addressed to J.W.

Reprints and permissions information is available at www.nature.com/reprints.

Publisher's note Springer Nature remains neutral with regard to jurisdictional claims in published maps and institutional affiliations.



Open Access This article is licensed under a Creative Commons Attribution 4.0 International License, which permits use, sharing, adaptation, distribution and reproduction in any medium or format, as long as you give appropriate credit to the original author(s) and the source, provide a link to the Creative Commons licence, and indicate if changes were made. The images or other third party material in this article are included in the article's Creative Commons licence, unless indicated otherwise in a credit line to the material. If material is not included in the article's Creative Commons licence and your intended use is not permitted by statutory regulation or exceeds the permitted use, you will need to obtain permission directly from the copyright holder. To view a copy of this licence, visit <http://creativecommons.org/licenses/by/4.0/>.

© The Author(s) 2022